Effects of temperature on the impedance of piezoelectric actuators used for SHM

Etienne Balmès, Mikhail Guskov, Marc Rebillat, Nazih Mechbal

Effects of temperature on the impedance of piezoelectric actuators used for SHM

Etienne Balmes[♯,♭1] , Mikhail Guskov[♯], Marc Rebillat[♯], Nazih Mechbal[♯]

[♯]*Arts et Metiers Paristech, PIMM, 151 boulevard de l'hôpital 75013, Paris, France*
[♭]*SDTools, 44 Rue Vergniaud 75013, Paris, France*

Highlights

- FEM modeling of piezoelectric patches used as actuators and sensors for SHM applications.
- Test/analysis correlation of temperature effects in piezoelectric materials and glue
- Numerical methods associated with the prediction of electric transfers.

1 Introduction

Composites have become the materials of choice of aircraft nacelles, since they are light and also provide effective acoustic protection. However, fiber reinforced materials are complex. Their structural anisotropy and the fact that they contain different phases of material (fibers and matrix) generally results in various types of damage with different propagation characteristics. Damage detection and determination of the remaining strength and life of the structure is challenging task called Structural Health Monitoring. SHM is a broad field encompassing many synergetic technologies that provide together automated systems whose purposes are to identify and characterize possible damage within structures, in real-time or at specified time intervals. Some recent surveys [4] have shown that even reluctant industry areas are now convinced that SHM is the key technology to enable the transition from traditional schedule-driven maintenance to condition-based maintenance.

Among different actuation/sensing technologies piezoelectric patches are often considered for SHM applications. When using such patches to generate high frequency waves to be used as SHM indicators, understanding possible variations of the coupling properties is critical. Such variations can be associated with changes in the instrumented structure which is the target of SHM applications, but also variations of glue properties, degradation of the bonding or of the patches themselves. Numerical simulations, when predictive, give the ability to understand the relative effects of property changes such as temperature and damage in much more detail than test and are thus quite fundamental for design. Key challenges addressed in the present modeling effort are thus validation of models by correlation, introduction of model reduction technique to handle high frequency responses, introduction of parametric studies where the effects of changing parameters can be understood.

Section 2 addresses modeling introducing equations of motion and electrical boundary conditions. Section 3 then discusses solution strategies for the efficient computation of electrical transfers and illustrates these methods for the case of a rectangular patch showing the main features of static capacity and in-plane resonance frequency [1]. A "snapshot" reduction strategy is proposed and shown to correctly capture modes with an electrical impact in a wide frequency range with many structural modes, but few actually visible in the electrical transfer. Numerical conditioning issues are also discussed.

The first test/analysis correlation is performed on an isolated patch and confirms the effect of the sensitivity of permittivity to temperature on static capacity but not on the in-plane resonance. Section 4 then investigates the effect of temperature on a composite equipped with a patch. The tests available clearly illustrate that for high enough temperatures, the stiffness of epoxy may drop enough to reach a configuration, where the patch behaves almost as uncoupled to the composite. The same effect is well reproduced by the model thus confirming its validity.

[1]Corresponding author: +33.1.44.24.63.71 – *prenom.nom@ensam.eu – http://pimm.paris.ensam.fr*

2 Equations of motion

Starting from piezoelectric constitutive laws piezoelectric volume or shell elements can be formulated and lead to equations for the form [2, 3, 5]

$$\begin{bmatrix} M_{qq}s^2 + K_{qq} & K_{qV} \\ K_{Vq} & K_{VV} \end{bmatrix} \begin{Bmatrix} q_{mech} \\ V \end{Bmatrix} = \begin{bmatrix} Z_{CC}(s) & Z_{CV} \\ Z_{VC} & Z_{VV} \end{bmatrix} \begin{Bmatrix} q_{mech} \\ V \end{Bmatrix} = \begin{Bmatrix} F_{mech} \\ Q \end{Bmatrix} \tag{1}$$

where $\{q_{mech}\}$ contains the mechanical degrees of freedom (translations u, v, w and rotations for shells), $\{V\}$ contains the electric potential degrees of freedom, $\{F_{mech}\}$ is the vector of applied external mechanical forces, and $\{Q\}$ is the vector of applied external charges. Volumes use one electrical DOF per node giving the electric potential and an equipotentiality constraint is added. For the current formulation of shells, a single DOF giving the difference of potential between the two electrodes is used with no need for additional constraint.

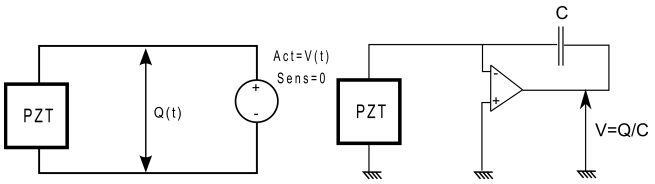

Figure 1: Closed circuit: voltage actuator, charge sensor

Short circuit (SC), charge sensors configurations correspond to cases where the potential is forced to zero (the electrical circuit is shorted). In (1), this corresponds to a case where the potential (electrical DOF) is fixed and the charge corresponds to the resulting force associated with this boundary condition. A **voltage actuator** corresponds to the same problem with $V = V_{In}$. The closed circuit charge is associated with the constraint on the enforced voltage and can be computed by extracting the second row of (1)

$$\{Q\} = [Z_{VC}]\{q_{mech}\} + [Z_{VV}]\{V_{In}\} \tag{2}$$

SC is the boundary condition used in a FEM model when voltage is the input (voltage actuation). The frequencies of the associated modes will be visible in the response. The alternative is to leave the potential free which corresponds to not specifying any boundary condition.

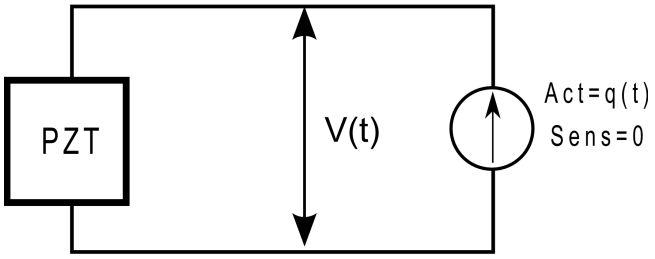

Figure 2: Open circuit (voltage sensor, charge actuator)

Open circuit (OC), voltage sensor, configurations correspond to cases where the total charge on the electrodes remains zero and a potential is created on the electrodes due to mechanical deformations. A piezoelectric actuator driven using a charge source also would correspond to this configuration (but the usual is voltage driving).

The voltage DOF $\{V\}$ associated to open-circuits are left free in (1). Since electrostatics are normally considered, Z_{vv} is actually frequency independent and the voltage DOFs could be condensed exactly

$$\{V\} = [Z_{VV}]^{-1}\left(Q_{in} - [Z_{VC}]\{q_{mech}\}\right) \tag{3}$$

Since voltage is an explicit DOF, it can be observed in DOF. Similarly charge is dual to the voltage, so a charge input is a simple point load on the active DOF associated to an electrode. Note that specifying a charge distribution (but not a total charge) does not make sense since you cannot both enforce the equipotential condition and specify a charge distribution that results from this constraint.

It is possible to observe charge in an OC condition, but this is of little interest since this charge will remain at 0.

3 Numerical prediction of electromechanical signatures

The terminology "electro-mechanical signature" of piezoelectric elements encompass different physical meanings depending on the application goal: damage detection or sensor diagnostics. All of them are however based on the measure of electrical properties in a piezoelectric.

Assuming a voltage driven actuation, the closed circuit condition is found, and physical poles are found as the result of the eigensolution of (1) with $V = 0$. The associated poles are called physical in the sense that the transfer between any load (mechanical or charge) and any response will use these same poles, while zeroes will change for each actuator/sensor pair. Physical poles are always fairly stable for small property changes, whereas zeroes can be significantly modified changes in the observation, which tends to be more easily modified.

One will here in particular focus on the dynamic capacity $C(s) = Q/V$. The impedance V/I often considered in the literature is not retained here since it is given by $1/sC(s)$ and thus shows poles that do not correspond to modes of the structure but zeroes of the admittance ($Y = sC(s)$).

As shown in Fig 3, the dynamic capacity has a low frequency asymptote. This static capacity is a common metric for sensor diagnostic and SHM [6, 9, 10, 7, 8], where one computes the average over a low frequency band of the real part of the dynamic capacity

$$C^S = \frac{1}{\omega_b - \omega_a} \int_{\omega_a}^{\omega_b} Re(C(i\omega))d\omega \tag{4}$$

The dynamic capacity also presents resonances which, for basic geometries, are well documented in [1]. For the rectangular patch shown here (28x14mm MFC M-2814-P1 from Smart Materials in d3x actuation), the first mode is a transverse mode along the length or in-plane traction mode. The second mode in-plane mode is then also visible in the computed capacity. For this fairly simple case, the first in-plane mode is mode 26, while the second corresponds to mode 49. Other modes, whose frequencies are shown as vertical lines, are bending modes that are not electrically visible (controllable by voltage or observable in the charge).

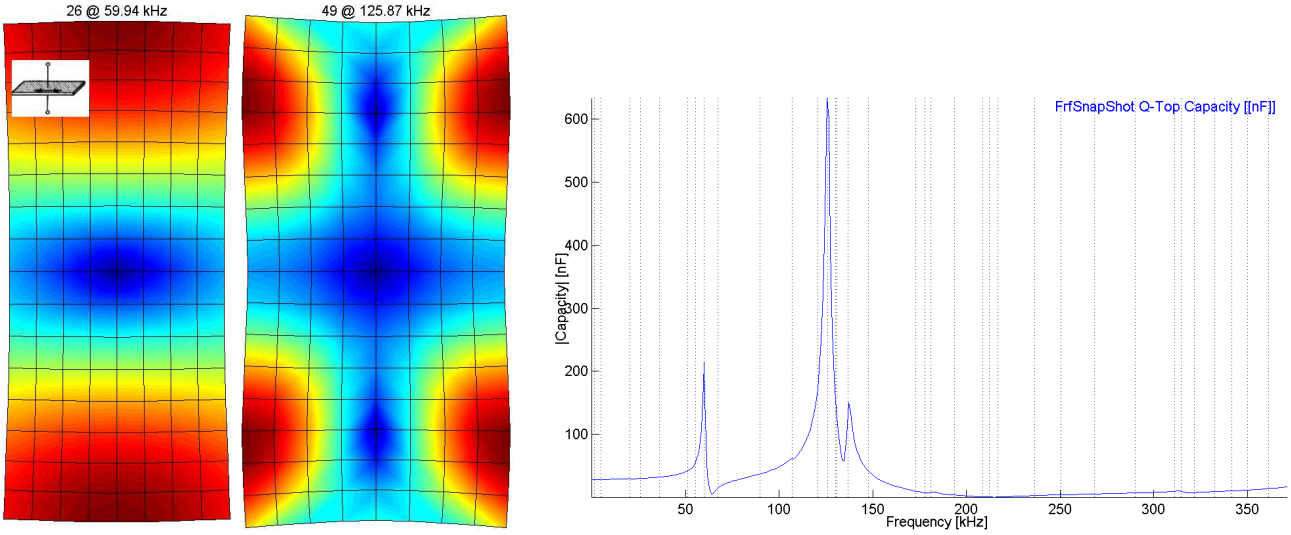

Figure 3: a) Computed modes of a rectangular patch and expected first mode [1], b) dynamic capacity

From a numerical point of view, guaranteeing the computation of a sufficient number of modes to properly represent the dynamic capacity can be a significant challenge. Using static correction to complement short circuited modes, that is computing using a basis of the form

$$T = \left[\begin{array}{cc} \phi(Zcc(\omega_j)) & K_{CC}(s)^{-1}K_{CV}(s)V_{In} \\ 0 & V_{In} \end{array} \right]_{\perp M,K} \tag{5}$$

is a first requirement. This guarantees that the static capacity is found exactly. The selection of dynamic modes can however be an important problem. In Fig 4a it clearly appears that computing a 100 modes, shown as circular markers in Fig 4, gives a model that barely goes over 300 kHz. The last visible resonance corresponds to the shape associated with the static correction.

To avoid the need to compute a very large number of modes, a novel "snapshot" reduction strategy is proposed here. One first computes the dynamic response (1) at a set of target frequencies, typically 20 regularly spaced in the target frequency interval. One then builds a Ritz basis by computing a mass orthonormal and stiffness orthogonal basis T for

the subspace generated by these responses

$$T = \left[\left\{ \begin{array}{c} Z_{CC}(s)^{-1} Z_{CV}(s) V_{In} \\ V_{In} \end{array} \right\}_{s \in i\omega_{target}} \right]_{\perp M,K} \tag{6}$$

Using a Rayleigh Ritz procedure, one finally computes the response as a linear combination of the vectors T.

Fig 4b shows that the snapshot reduction method gives very similar results in up to 300 kHz but captures additional in-plane modes correctly at higher frequencies. The resonances visible in the electrical response are all correctly captured while the low frequency bending modes are not found. The validity of this method can be clearly related to that of subspace identification methods [11], where identifiable modes of a system are captured by generating a response associated with a specific excitation.

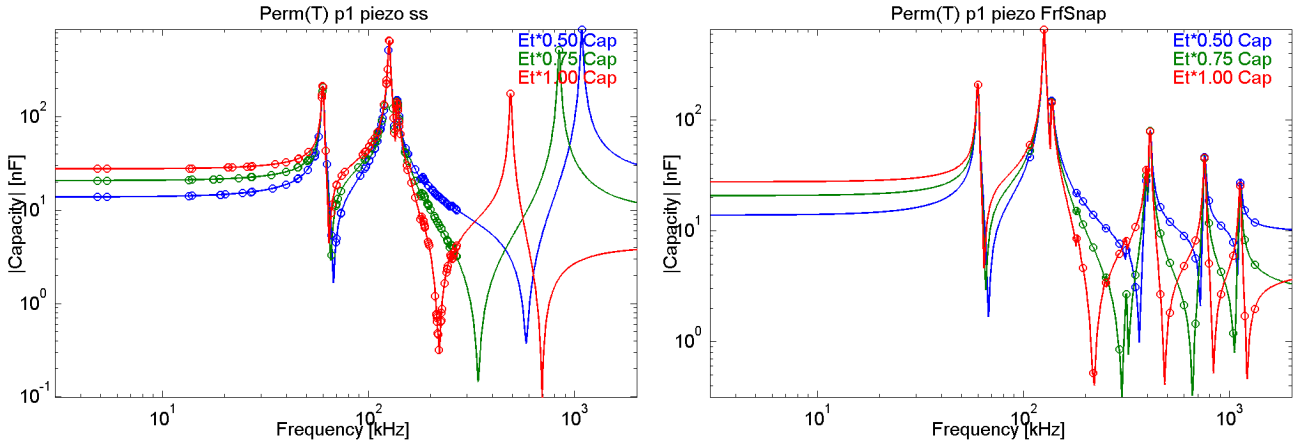

Figure 4: Influence of permittivity on dynamic capacity a) modal model with 100 modes and static correction, b) snapshot reduction

Figure 5 illustrates the evolution of the dynamic capacity as a function of frequency and temperature for an isolated circular patch from Noliac (shown in Fig 7b, but not bonded). The static capacity clearly shows a strong increase with temperature. To analyze the relation with model properties, Fig 5 shows the evolution of the dynamic capacity under a change of the permittivity at zero stress ϵ^T. It clearly appears that the experimental change in static capacity is directly related to the change in permittivity. The visible resonances correspond to in-plane modes as for the rectangular patch in Fig 3. Since the elastic constants of the model are unchanged and the electrical boundary condition is a short circuit, the frequencies are not affected. The slight variation of frequency visible in the experiment thus indicates elastic properties have a slight dependence on temperature.

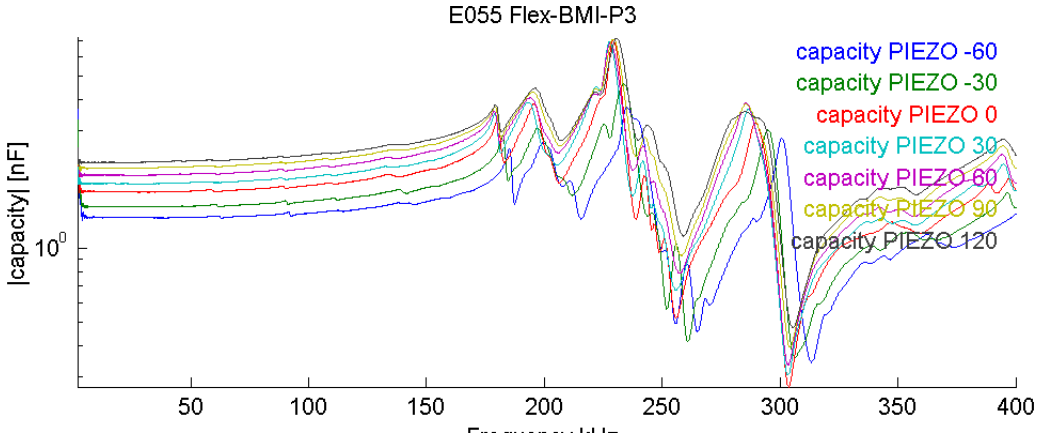

Figure 5: Experimental characterization of the influence of temperature on the dynamic capacity of a circular patch

When using classical units, the scaling of Z_{vv} can be quite different of that of Z_{cc}. Depending on the sparse solver used, one may obtain results that are quite incorrect on the prediction of the electrical field. Fig 6 thus illustrates two computations performed using the PARDISO sparse solver with and without preconditioning. Clearly, only the preconditioned result is correct and it seems that problems in earlier results were associated with this conditioning issue.

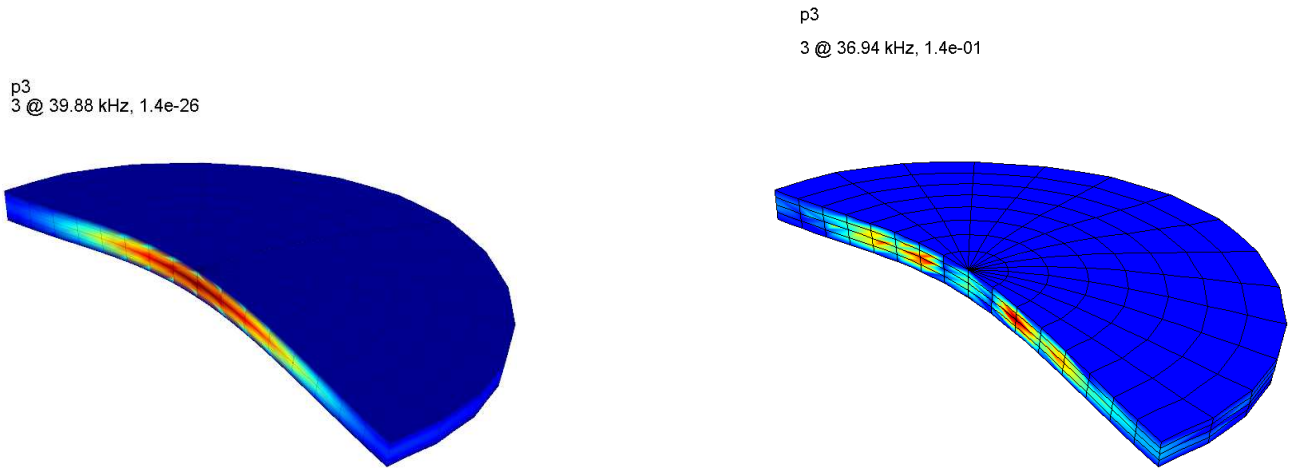

Figure 6: Sample round-off error on predicted electrical field. (a) correct result obtained with pre-conditioning. (b) round-off error leading to irregular electrical field

4 Effects of temperature for composite equipped with patches

For SHM applications, the patches are glued to a structure which in the present work is a monolithic composite. To account for material properties in detail, one considers a volume mesh distinguishing an orthotropic base plate, shown in blue in Fig 7, a glue layer 302-3M produced by EPO-TEK assumed to be an isotropic elastic material, in orange, and an transversely isotropic piezoelectric material shown in green. The electrodes are placed on the circular surfaces and polarization is in the 33 direction normal to the surface.

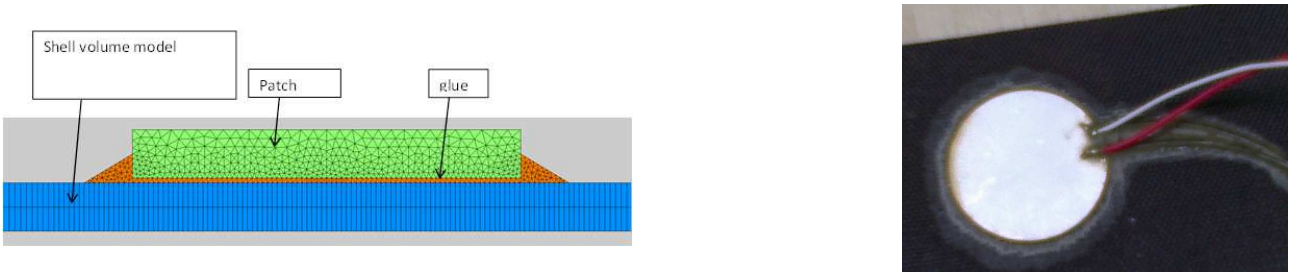

Figure 7: (a) sample mesh with glue. (b) Actual patch

The experimental result in Fig 8a clearly indicates a significant evolution of resonance frequencies as the temperature rises. At 120 C, the measured capacity is actually almost overlaid with the isolated patch measurement shown in thick dashed lines. As before, the change in permittivity explains the shift of static capacity but does not explain shifts of resonances. The assumption made is that the most important effect of temperature is a decrease in the glue modulus as this is consistent with the known viscoelastic behavior of the glue.

To get a better understanding of glue effects, one considers a range of glue moduli between Eg=0.1 GPa to 4 GPa for the smaller P3 patch. Fig 8b shows that the main resonance mode is near 250 kHz for a soft glue and increase up to 350 kHz for a stiff one. The transition is smooth and the level of contribution of lower frequency flexible modes decreases as the glue modulus decreases. This is clearly consistent with the idea that for low glue stiffness the level of coupling between the piezo and the laminate becomes fairly low.

5 Conclusion

FEM models and associated numerical solution strategies were introduced and shown allow correct predictions of dynamic capacity and its evolution with temperature in both isolated and glued configurations. The model clearly gives all the expected trends so that one can imagine using it to solve inverse problems and thus characterize the sensitivity of material properties (permitivity and moduli) to temperature through inverse problems. Obtaining a validated temperature dependent model will allow to optimize sensor configurations in terms of key SHM processes. In particular sensor self-diagnostic through the use of electrical impedance measurements and use of patches to generate Lamb waves for detection should be validated in the presence of unknown temperature variations.

Acknowledgments

This study was partially funded by the CORAC/EPICE project CORALIE.

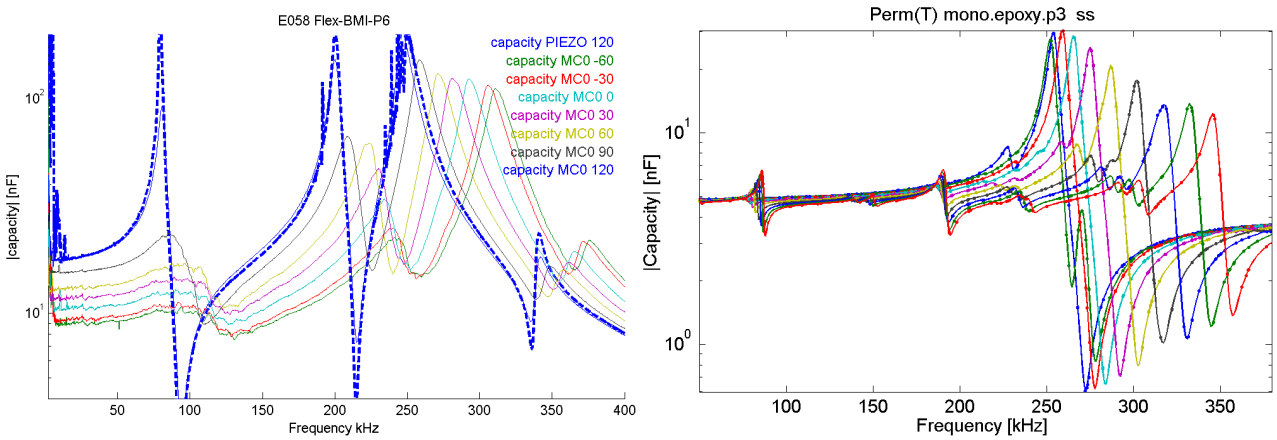

Figure 8: (a) Influence of temperature capacity 25 mm diameter P6 disk. (b) Influence of glue modulus for 8 mm P3 disk.

References

[1] Piezoelectric properties of ceramic materials and components. part 2: methods of measurement low power. *European standard 50324*, 2002.

[2] E. Balmes and A. Deraemaeker. *Modeling structures with piezoelectric materials, SDT tutorial*. SDTools, 2013.

[3] Etienne Balmes and Corine Florens. Validation of a vibration and electric model of honeycomb panels equipped with piezoelectric patch actuators. *Revue des composites et des matériaux avancés*, 19(3):319–338, 2009.

[4] F.-K. Chang. Structural Health Monitoring: Condition-based Maintenance. In *Proc. 8th International Workshop on Structural Health Monitoring (IWSHM), Stanford*, 2011.

[5] Corine Florens. *Modeling of the viscoelastic honeycomb panel equipped with piezoelectric patches in view of vibroacoustic active control design*. PhD thesis, École Centrale Paris, 2009.

[6] V. Giurgiutiu and A. N. Zagrai. Embedded self-sensing piezoelectric active sensors for on-line structural identification. *Journal of Vibration and Acoustics-transactions of the Asme*, 124(1):116–125, January 2002.

[7] B. L. Grisso and D. J. Inman. Temperature corrected sensor diagnostics for impedance-based shm. *Journal of Sound and Vibration*, 329(12):2323–2336, June 2010.

[8] K. R. Mulligan, N. Quaegebeur, P. C. Ostiguy, P. Masson, and S. Letourneau. Comparison of metrics to monitor and compensate for piezoceramic debonding in structural health monitoring. *Structural Health Monitoring-an International Journal*, 12(2):153–168, March 2013.

[9] G. Park, C. R. Farrar, A. C. Rutherford, and A. N. Robertson. Piezoelectric active sensor self-diagnostics using electrical admittance measurements. *Journal of Vibration and Acoustics-transactions of the Asme*, 128(4):469–476, August 2006.

[10] S. Park, G. Park, C. B. Yun, and C. R. Farrar. Sensor self-diagnosis using a modified impedance model for active sensing-based structural health monitoring. *Structural Health Monitoring-an International Journal*, 8(1):71–82, January 2009.

[11] P. Van Overschee and B. De Moor. *Subspace identification for linear systems*. Kluwer academic press, 1996.